



# Quality assessment of CNES real-time ionospheric products

Zhixi Nie<sup>1</sup> · Hongzhou Yang<sup>1</sup> · Peiyuan Zhou<sup>1</sup> · Yang Gao<sup>1</sup> · Zhenjie Wang<sup>2</sup>

Received: 31 July 2018 / Accepted: 9 November 2018 / Published online: 15 November 2018  
© Springer-Verlag GmbH Germany, part of Springer Nature 2018

## Abstract

Real-time single-frequency precise point positioning (RT-SF-PPP) has become a desired positioning approach because it can achieve high positioning accuracy with a low-cost global navigation satellite system (GNSS) chipset or receiver. For single-frequency precise point positioning (SF-PPP) applications, the ionospheric delay is a dominant error source, and thus the quality of applied ionospheric products is critical to the performance of SF-PPP. To meet the demands of the RT-SF-PPP users, the international GNSS service (IGS) is planning to provide open-access real-time ionospheric products. By now, the Centre National d'Études Spatiales (CNES) is the only IGS analysis center (AC) to broadcast real-time ionospheric vertical total electron content (VTEC) message through its real-time service (RTS). The quality of the CNES real-time ionospheric products is drawing increasing attention from the GNSS community. We evaluate the quality of CNES real-time VTEC message both in the ionospheric correction domain and positioning domain. First, 374 consecutive days of CNES VTEC products are collected and compared with the IGS final global ionospheric map (GIM) products. Second, slant total electron content (STEC) computed with CNES VTEC message is fully assessed with respect to STEC derived from dual-frequency GNSS measurements. Finally, RT-SF-PPP is conducted for assessing the quality of CNES real-time ionospheric products in the positioning domain. The degree and order of the spherical harmonic expansions broadcasted in the CNES VTEC messages changed from 6 to 12 in the time span of collected data, the effects of higher degree and order parameters are investigated at the same time in the experiments above.

**Keywords** Real time · SF-PPP · CNES · VTEC · STEC

## Introduction

Precise point positioning (PPP) is attractive to the global navigation satellite system (GNSS) community as a popular absolute positioning technology, because it can achieve high precision with a single GNSS receiver using precise satellite orbit and clock products (Bisnath and Gao 2009; Choy et al. 2017; Zumberge et al. 1997). Since 2013, the international GNSS service (IGS) has been providing an open-access real-time service (RTS), which includes real-time orbit, clock and other corrections. The advent of RTS corrections allows users to carry out real-time PPP. According to the standard of Radio Technical Commission for Maritime Services

(RTCM), RTS corrections are formatted into state space representation (SSR) messages (RTCM Special Committee 2016), and these messages are broadcasted over the internet based on Networked Transport of RTCM via Internet Protocol (NTRIP) (Weber et al. 2007). In the blueprint of IGS, the SSR messages are designed in three major stages (RTCM Special Committee 2016):

Step 1: The development of correction messages for satellite orbit, clock and code bias. This will enable real-time dual-frequency precise point positioning (RT-DF-PPP).

Step 2: The development of the ionospheric vertical total electron content (VTEC) message. This will enable real-time single-frequency precise point positioning (RT-SF-PPP).

Step 3: The development of messages for slant total electron content (STEC), tropospheric correction, and satellite phase biases. This will enable PPP-RTK, which is a fast integer ambiguity resolution-enabled precise point positioning (Teunissen and Khodabandeh 2015), for both dual- and single-frequency users.

✉ Hongzhou Yang  
honyang@ucalgary.ca

<sup>1</sup> Schulich School of Engineering, University of Calgary, Calgary, Canada

<sup>2</sup> School of Geosciences, China University of Petroleum, Qingdao, China

Currently, the SSR message types provided by most IGS analysis centers (ACs) only cover the first stage of RT-DF-PPP. The quality of IGS real-time products, mainly comprised of real-time orbit and clock correction, has been assessed by Hadas and Bosy (2015), Nie et al. (2018), Kazmierski et al. (2018), and Wang et al. (2018). The accuracy of real-time GPS orbit correction is about 3–5 cm, and the real-time GPS clock correction has a standard deviation of 0.1–0.15 ns. Hence, it is able to achieve centimeter to decimeter level with RT-DF-PPP. However, the high price of dual-frequency GNSS receiver is a major concern for a wide range of applications.

In recent years, RT-SF-PPP has begun to receive increasing interests, as it can achieve decimeter to sub-meter level positioning accuracy with a low-cost GNSS chipset or receiver (de Bakker and Tiberius 2017; Gao et al. 2006; van Bree and Tiberius 2012). However, the performance of RT-SF-PPP depends highly on the elimination of ionospheric delays (Choy 2009; Shi et al. 2012). To date, only one of IGS AC, the Centre National d'Études Spatiales (CNES), is broadcasting VTEC message, along with orbit, clock, code bias and phase bias messages, through its four RTS streams CLK90, CLK91, CLK92, CLK93. Among the four CNES streams, the orbits of CLK90 and CLK92 are referred to the center of mass, while those of CLK91 and CLK93 are referred to the antenna phase center. RT-SF-PPP can be carried out with CNES VTEC and other messages for single-frequency users. Roma et al. (2016) presented the initial results of the CNES VTEC products over 15 days. However, as of now, there is no literature devoted to the comprehensive quality assessment of the CNES real-time ionospheric products. We fill the gap in this contribution. In the following, the method to calculate ionospheric correction with CNES VTEC message is presented. Then, the quality of real-time ionospheric products is evaluated using three methods: (1) direct comparison with the IGS final global ionospheric map (GIM) products, (2) comparison between the STECs computed with CNES VTEC message and those derived from dual-frequency GNSS measurements and (3) performance analysis of RT-SF-PPP. Summaries and conclusions are provided in the last section.

### Ionospheric correction calculation with CNES VTEC message

According to the RTCM-SSR standard, the ionospheric VTEC is presented with one or multiple infinitesimal thin VTEC layers. The VTEC model at each layer is defined as spherical harmonic expansions, which allows characterizing a global and continuous VTEC representation. A spherical earth model is adopted.

The VTEC value, expressed in total electron content units (TECU), is computed for each layer as (RTCM Special Committee 2014)

$$VTEC(\varphi_{IPP}, \lambda_S) = \sum_{n=0}^N \sum_{m=0}^{\min(n,M)} (C_{n,m} \cos m\lambda_S + S_{n,m} \sin m\lambda_S) P_{n,m}(\sin \varphi_{IPP}), \tag{1}$$

where  $N$  and  $M$  are the degree and order of the spherical harmonic expansions;  $n$  and  $m$  denote the corresponding indices;  $C_{n,m}$  and  $S_{n,m}$  are the cosine and sine coefficients for the layer (unit: TECU);  $\varphi_{IPP}$  is the geocentric latitude of ionospheric pierce point (IPP) for the layer (unit: radian);  $\lambda_S$  denotes the mean sun-fixed and phase-shifted longitude of IPP for the layer (unit: radian);  $P_{n,m}(\cdot)$  is the fully normalized associated Legendre function. The mean sun-fixed and phase-shifted longitude  $\lambda_S$  is given by

$$\lambda_S = (\lambda_{IPP} + (t - 50, 400) * \pi/43, 200), \tag{2}$$

where  $\lambda_{IPP}$  is the longitude of IPP for the layer (unit: radian);  $t$  is the GPS time of computation epoch (unit: s). The approximate TEC maximum typically appears at local time 14:00 for which  $t = 50400s$ , and the longitude of the IPP is rotated by  $(t - 50, 400) * \pi/43, 200$  around the earth polar-axis to compensate to the strong correlation between VTEC and the sun's position.

The position of the IPP is defined to be the intersection of a straight line, from the user's location to the satellite, and a sphere with the height of the ionospheric layer above the spherical earth surface. First, the geocentric latitude is computed in radians according to

$$\varphi_{IPP} = \sin^{-1}(\sin \varphi_U \cos \psi_{IPP} + \cos \varphi_U \sin \psi_{IPP} \cos A), \tag{3}$$

where  $\varphi_U$  is the geocentric latitude of the user location (unit: radian);  $A$  denotes the azimuth of the satellite with respect to the user location (unit: radian);  $\psi_{IPP}$  is the spherical earth's central angle between the user location and the projection of the IPP to the spherical earth surface, it can be written in radians as

$$\psi_{IPP} = \frac{\pi}{2} - E - \sin^{-1}\left(\frac{R_e + h_U}{R_e + h_I} \cos E\right), \tag{4}$$

where  $E$  is the elevation angle of the satellite with respect to the user location (unit: radian);  $R_e$  is the spherical earth radius of 6370 km;  $h_U$  and  $h_I$  represent the heights of the user location and the ionospheric layer above the spherical earth surface (unit: km).

The longitude of the IPP in radians is computed as

$$\text{If } \varphi_U > 0 \text{ and } \tan \psi_{IPP} \cos A > \tan\left(\frac{\pi}{2} - \varphi_U\right).$$

$$\text{or } \varphi_U < 0 \text{ and } -\tan \psi_{IPP} \cos A > \tan\left(\frac{\pi}{2} + \varphi_U\right)$$

$$\lambda_{IPP} = \lambda_U + \pi - \sin^{-1} \left( \frac{\sin \psi_{IPP} \sin A}{\cos \varphi_{IPP}} \right). \tag{5}$$

Otherwise,

$$\lambda_{IPP} = \lambda_U + \sin^{-1} \left( \frac{\sin \psi_{IPP} \sin A}{\cos \varphi_{IPP}} \right), \tag{6}$$

where  $\lambda_U$  is the longitude of the user location (unit: radian).

The fully normalized associated Legendre functions can be computed with the following recursive formulas (Holmes and Featherstone 2002):

$$P_{n,n}(\sin \varphi_{IPP}) = \sqrt{\frac{2n+1}{2n}} \cos \varphi_{IPP} P_{n-1,n-1}(\sin \varphi_{IPP}), \quad n \geq 2 \tag{7}$$

$$P_{n,n-1}(\sin \varphi_{IPP}) = \sqrt{2n+1} \sin \varphi_{IPP} P_{n-1,n-1}(\sin \varphi_{IPP}), \quad n \geq 1 \tag{8}$$

$$P_{n,m}(\sin \varphi_{IPP}) = a_{n,m} \sin \varphi_{IPP} P_{n-1,m}(\sin \varphi_{IPP}) + b_{n,m} P_{n-2,m}(\sin \varphi_{IPP}), \quad 0 \leq m \leq n-2 \text{ and } n \geq 2 \tag{9}$$

where

$$a_{n,m} = \sqrt{\frac{(2n-1)(2n+1)}{(n-m)(n+m)}}, \tag{10}$$

$$b_{n,m} = \sqrt{\frac{(2n+1)(n+m-1)(n-m-1)}{(n-m)(n+m)(2n-3)}}. \tag{11}$$

The sectoral  $P_{n,n}(\sin \varphi_{IPP})$  are computed with (7) using the starting values  $P_{0,0}(\sin \varphi_{IPP}) = 1$  and  $P_{1,1}(\sin \varphi_{IPP}) = \sqrt{3} \cos \varphi_{IPP}$ , these sectoral values can serve as seeds for the forward column recursions in (8) and (9). The complete recursion process is explained as Fig. 1,

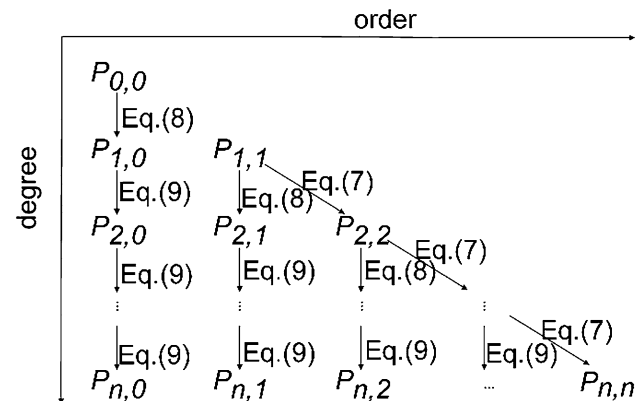


Fig. 1 Schematic diagram of the recursion employed in fully normalized associated Legendre function computations

the degree increases in rows down, the order increases in columns to the right, the direction of arrowhead represents forward computation, and the corresponding recursive formula is given aside.

Once the VTEC of the specific IPP is obtained, the STEC of the layer  $i$  can be computed with the VTEC value divided by the mapping function

$$STEC_i = \frac{VTEC_i}{\cos Z_{IPP}} = \frac{VTEC_i}{\sin(E + \psi_{IPP})}, \tag{12}$$

where  $Z_{IPP}$  is the zenith distance of the satellite with respect to the IPP. The total STEC is the sum of the individual STEC contribution of each layer, and the ionospheric correction in meters of a specific frequency  $f$  (unit: Hz) is given by

$$IC = \pm \frac{40.3 \times 10^{16}}{f^2} STEC, \tag{13}$$

where positive sign applies for pseudorange observations and negative sign applies for phase range observations.

### Quality assessment

To assess the quality of real-time VTEC products provided by CNES, the real-time SSR messages mounted on CLK93 are received and decoded for 374 consecutive days, starting from June 22, 2017 to June 30, 2018. The solar activity is relatively mild during the selected period. For the CNES VTEC messages, the sample rate is 1 min and a single thin layer model is adopted with height of 450 km. Notice that, the degree and order of the spherical harmonic expansions broadcasted in the CNES VTEC messages changed from 6 to 12 in the time span of collecting data. Accordingly, the whole data are divided into two periods: Period 1 contains data from 06:35:00 June 22, 2017 to 07:58:00 May 29, 2018, of which the spherical harmonic degree and order are both 6; Period 2 includes data from 08:50:00 May 29, 2018 to 23:59:00 June 30, and the degree and order of the spherical harmonic expansions are both 12. In the following experiments, Periods 1 and 2 are evaluated separately to investigate the effects of higher degree and order parameters. Meanwhile, the availability of the VTEC products is also counted for the whole period. The available number of epochs is 524,075 and the missing number of epochs is 14,090, thus the availability of CNES VTEC messages is as high as 97.38% for 374 consecutive days from midyear 2017 to midyear 2018. Afterward, three sets of experiments

are carried out to evaluate the CNES VTEC products. First, the VTEC products are directly compared with the IGS final GIM products for both periods; second, the comparison is conducted regarding STEC, and the reference is the STEC derived from dual-frequency GNSS measurements. Last but not least, the performance of RT-SF-PPP with the CNES products is presented to investigate the product quality in positioning domain.

### Comparison with IGS final GIM products

The IGS final GIM is a combination of GIM products provided by individual IGS ACs, and has been systematically generated on a daily basis with a latency of approximately

11 days since 1998. The IGS final GIM is a VTEC grid dataset in IONosphere map Exchange (IONEX) format, with a resolution of 2 h, 5 degrees and 2.5 degrees in time, longitude and latitude, respectively (Feltens 2003; Hernández-Pajares et al. 2009, 2017). Previous research has shown that the IGS final GIM product is able to provide a high accuracy of 2–8 TECU VTEC grid (<http://www.igs.org/products>). To facilitate the direct comparison between the CNES real-time VTEC and IGS final GIM products, the CNES real-time GIM is produced with the same temporal and spatial resolution as IGS final GIM using CNES VTEC message. The same epochs in two consecutive days, 12:00:00 UT, May 28 of 2018 representing Period 1 and 12:00:00 UT, May 29 of 2018 representing Period 2, are selected to show the CNES

**Fig. 2** CNES real-time GIM (top) and IGS final GIM (bottom) at 12:00:00 UT, May 28 of 2018 (Unit: TECU)

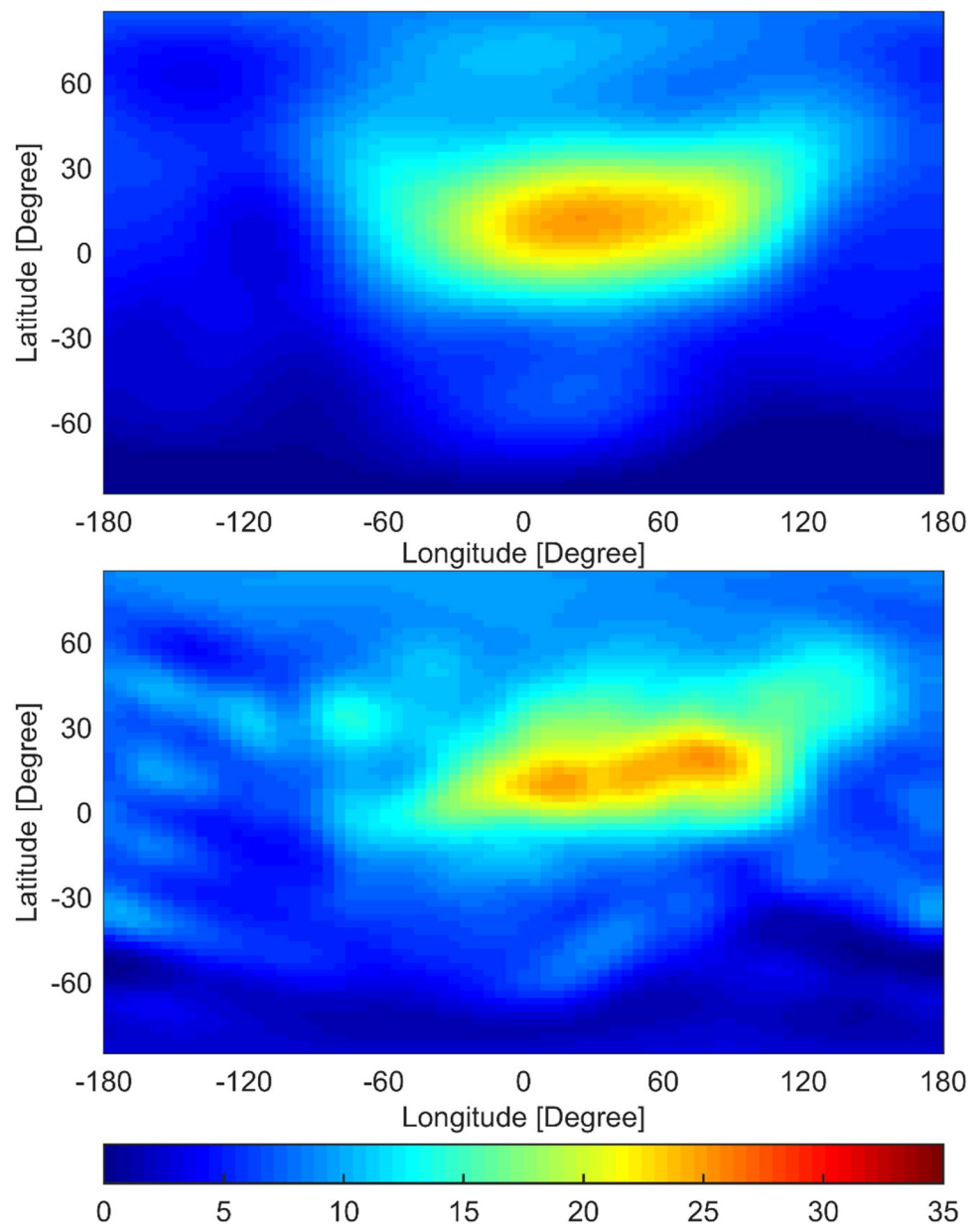
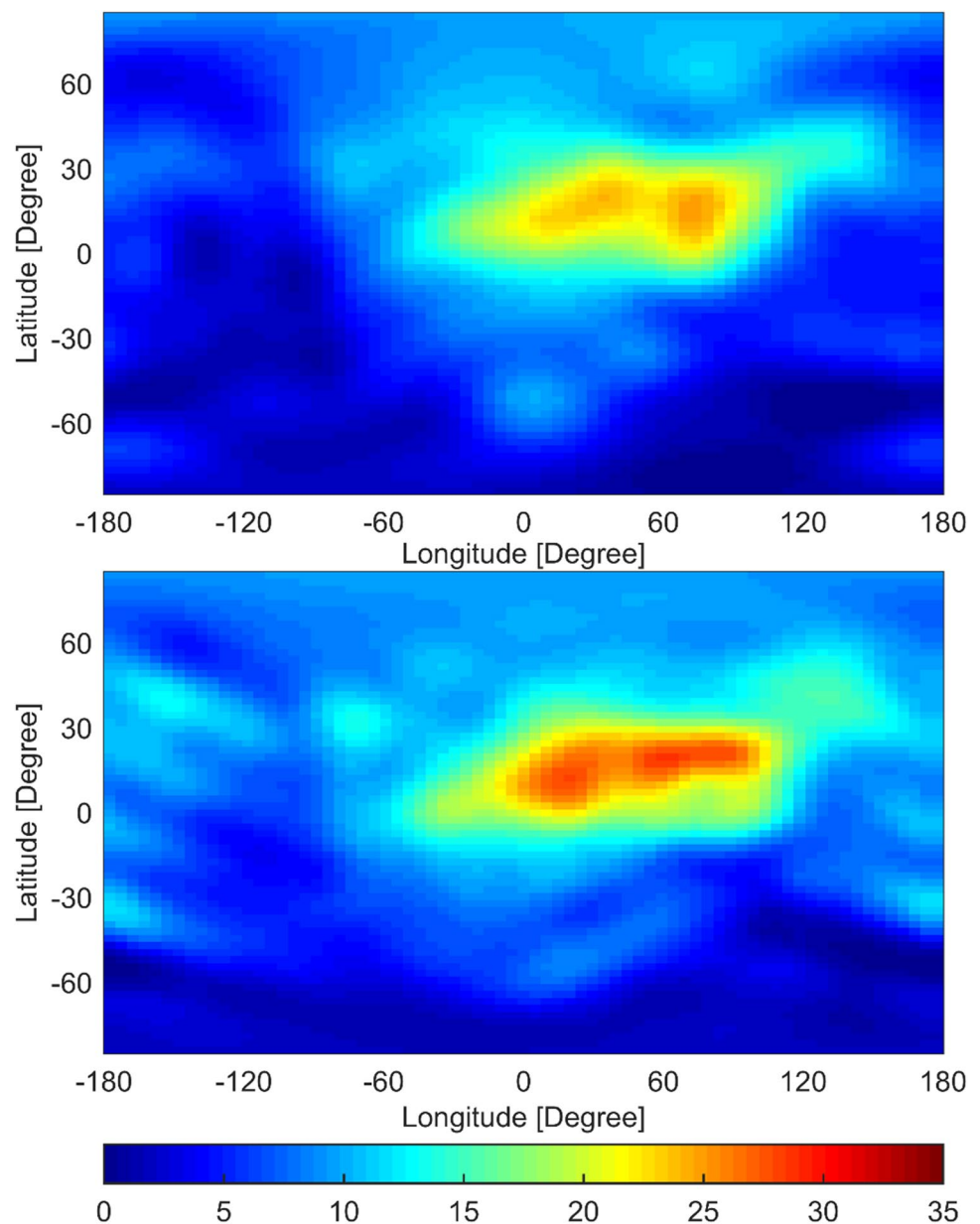


**Fig. 3** CNES real-time GIM (top) and IGS final GIM (bottom) at 12:00:00 UT, May 29 of 2018 (Unit: TECU)



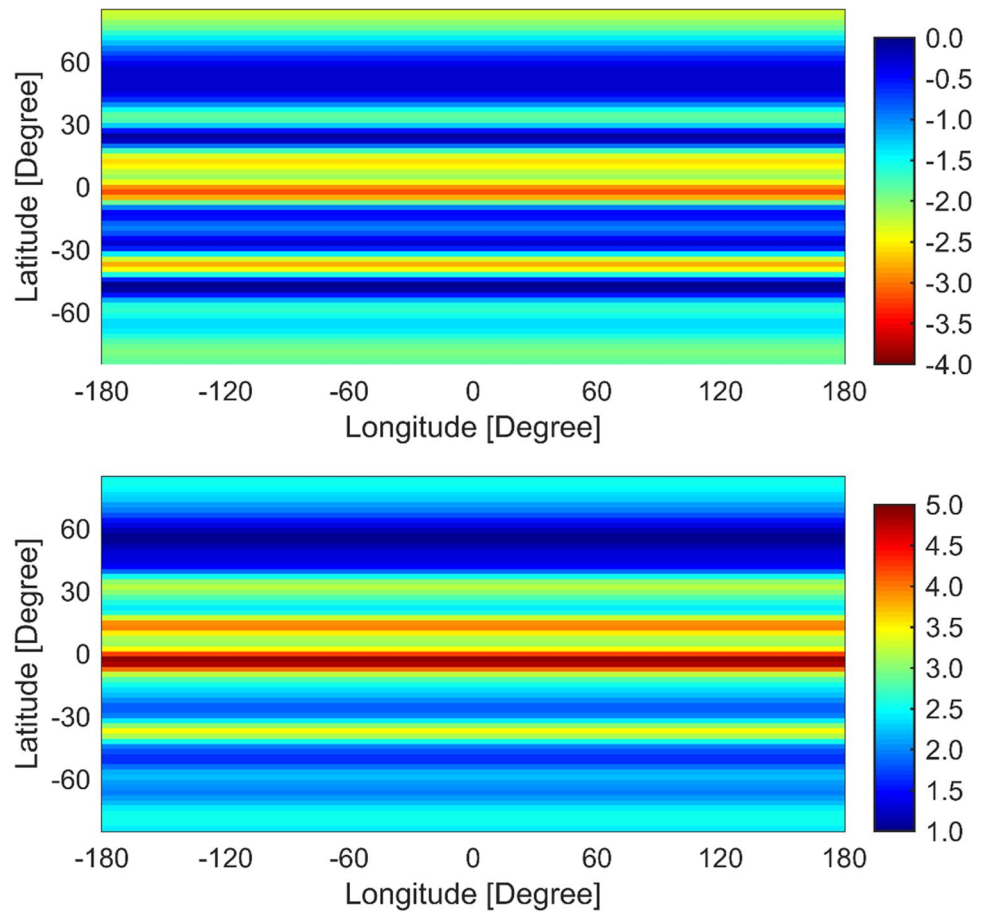
real-time GIM and IGS final GIM in Figs. 2 and 3. As we can see, both CNES real-time GIM and the IGS final GIM show clear diurnal and geographic feature. Meanwhile, the IGS final GIM shows more details compared to CNES real-time GIM, especially near the equatorial region. By comparing Figs. 2 and 3, we can see the CNES real-time GIM agrees better with IGS final GIM at 12:00:00 UT on May 29, 2018, which belongs to Period 2 with degree and order of the spherical harmonic expansions both at 12.

Afterward, the IGS final GIM is set as the reference and the error of CNES real-time VTEC products is assessed in terms of bias and RMS. The bias and RMS of CNES real-time VTEC products for Periods 1 and 2 are shown in Figs. 4 and 5, respectively. As we can see, the bias and RMS of

CNES real-time VTEC products show similar spatial feature, which consists of several horizontal stripes with different latitudes. For Period 1, the bias of CNES real-time VTEC varies from  $-3.15$  to  $-0.03$  TECU for different grid points, while the RMS varies from 1.06 to 4.91 TECU. As for Period 2, the bias varies from  $-2.82$  to  $0.06$  TECU, and the RMS varies from 0.97 to 3.01 TECU. By comparing the RMS of CNES real-time GIM between Period 1 and Period 2, we can see that CNES VTEC message with higher degree and order of the spherical harmonic expansions can improve the accuracy when taking IGS final GIM products as the reference, especially in low latitudes.

Apart from the spatial feature of the quality of CNES real-time VTEC products, the temporal performance analysis of the

**Fig. 4** Global maps of bias (top) and RMS (bottom) for CNES real-time VTEC products in Period 1 (Unit: TECU)



CNES real-time VTEC products is carried out as well. Both bias and RMS of CNES real-time VTEC products are computed over all grid points at each epoch for the 374 consecutive days. The time series of bias and RMS over 374 consecutive days are shown in Fig. 6, and the black vertical line separates the time span into Period 1 and Period 2. Additionally, the ionospheric Dst index (Campbell 1996), which can indicate the intensity of magnetic activity, is also included. Over the 374 consecutive days, the bias of CNES real-time VTEC products ranges from  $-4.36$  to  $0.86$  TECU, and the RMS of those varies from  $0.80$  to  $7.04$  TECU. Meanwhile, the correlation between the RMS values of the CNES real-time VTEC products and the Dst indexes is quite strong. The larger Dst, the less accurate CNES real-time VTEC products. Therefore, the CNES real-time VTEC products should be applied with cautious during intensive magnetic activities. It is also noted that the RMS of CNES real-time VTEC products decreases from Period 1 to Period 2. The higher the degree and order of the spherical harmonic expansions, the more accurate the CNES VTEC products.

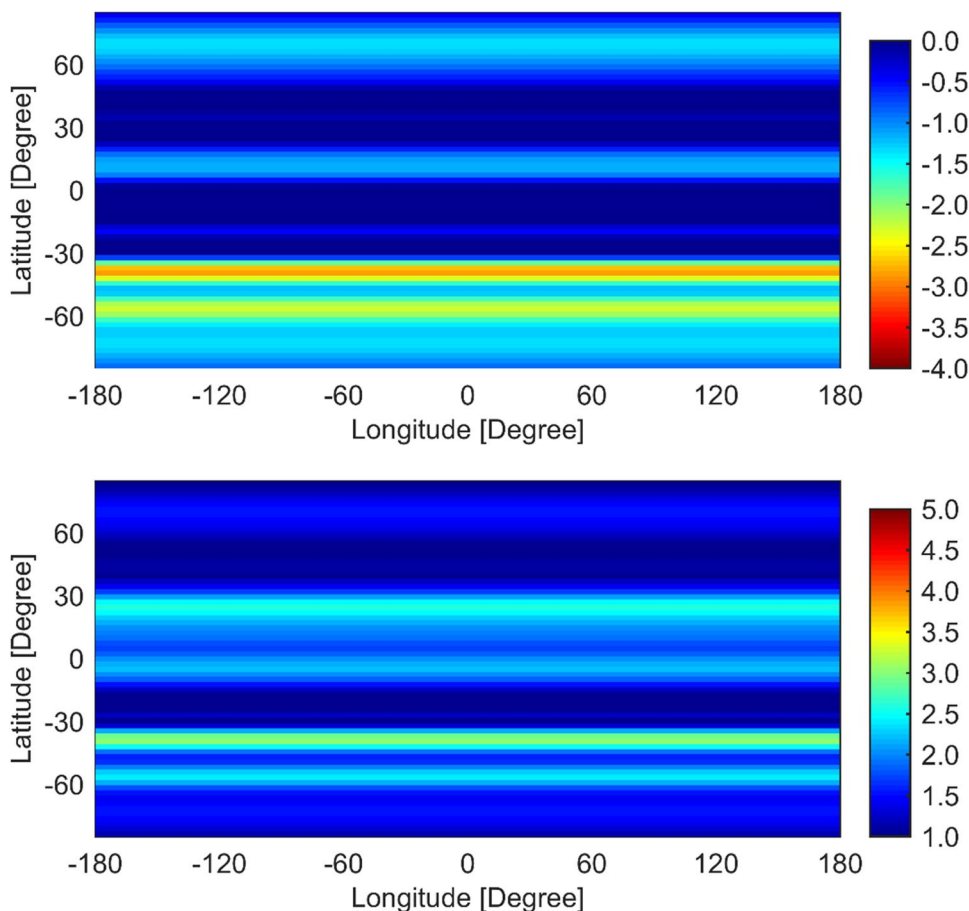
**Comparison with STEC derived from dual-frequency measurements**

The ionospheric combinations for code and phase can be written as (Bishop et al. 1985; Brunini and Azpilicueta 2009)

$$\begin{cases} PI = P_1 - P_2 = \gamma \cdot I_1 + c \cdot DCB_{r,P_1-P_2} + c \cdot DCB_{P_1-P_2}^s \\ LI = L_1 - L_2 = -\gamma \cdot I_1 + \lambda_1 N_1 - \lambda_2 N_2 \end{cases} \quad (14)$$

where  $P_i$  and  $L_i$  denote the raw code and phase observations,  $I_1$  represents the ionospheric delay at the first frequency,  $\gamma = 1 - f_1^2/f_2^2$  is the scale factor and  $f_i$  is the  $i$ th frequency value,  $\lambda_i$  and  $N_i$  are the wavelength and phase ambiguity at the  $i$ th frequency, respectively,  $c$  is the speed of light,  $DCB_{r,P_1-P_2}$  and  $DCB_{P_1-P_2}^s$  are the differential code biases at the receiver and satellite ( $i = 1, 2$ ). Given the poor precision of code measurements, the phase measurements are usually used for smoothing the code measurements. The phase-smoothed code ionospheric combination can be expressed as (Schaer 1999)

**Fig. 5** Global maps of bias (top) and RMS (bottom) for CNES real-time VTEC products in Period 2 (Unit: TECU)



$$\overline{PI}(t_n) = \frac{\sum_{i=1}^n (PI(t_i) + LI(t_i))}{n} - LI(t_n) = \gamma \cdot I_1 + c \cdot DCB_{r,P_1-P_2} + c \cdot DCB_{P_1-P_2}^s, \tag{15}$$

where  $LI(t_i)$ ,  $PI(t_i)$  are the phase and code ionospheric residual combinations at the epoch time  $t_i (i = 1, \dots, n)$ , and  $n$  is the number of smoothing epochs. The *STEC* derived from phase-smoothed code ionospheric combination is given by

$$STEC = \frac{f_1^2}{40.3 \times 10^{16}} I_1, \tag{16}$$

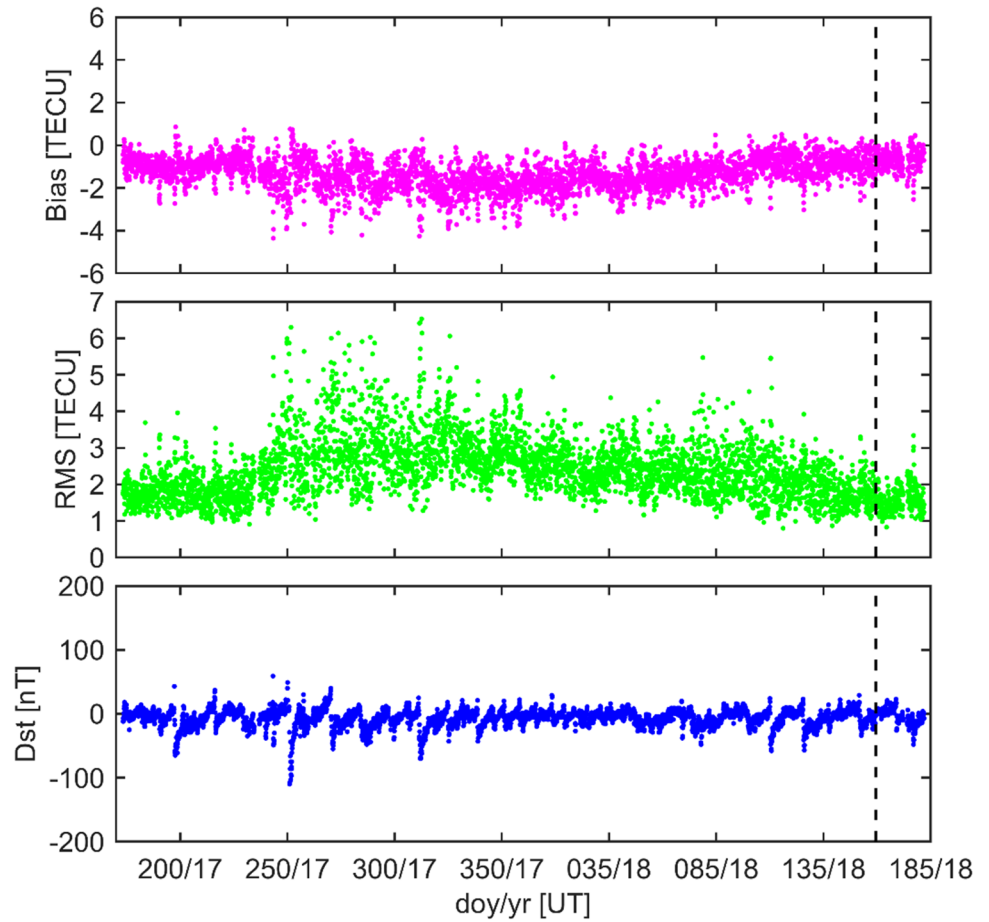
which can describe the ionospheric delay in the line of sight direction.

To implement the evaluation regarding *STEC*, 25 globally distributed IGS stations are selected and shown in Fig. 7. The GNSS raw data with a sample rate of 30 s are downloaded from June 22, 2017 to June 30, 2018 from IGS ftp server. However, only GPS measurements are used to calculate the *STEC*. The *STEC* derived from phase-smoothed code ionospheric combination is used as the reference, and then the *STEC* to be evaluated is calculated with CNES

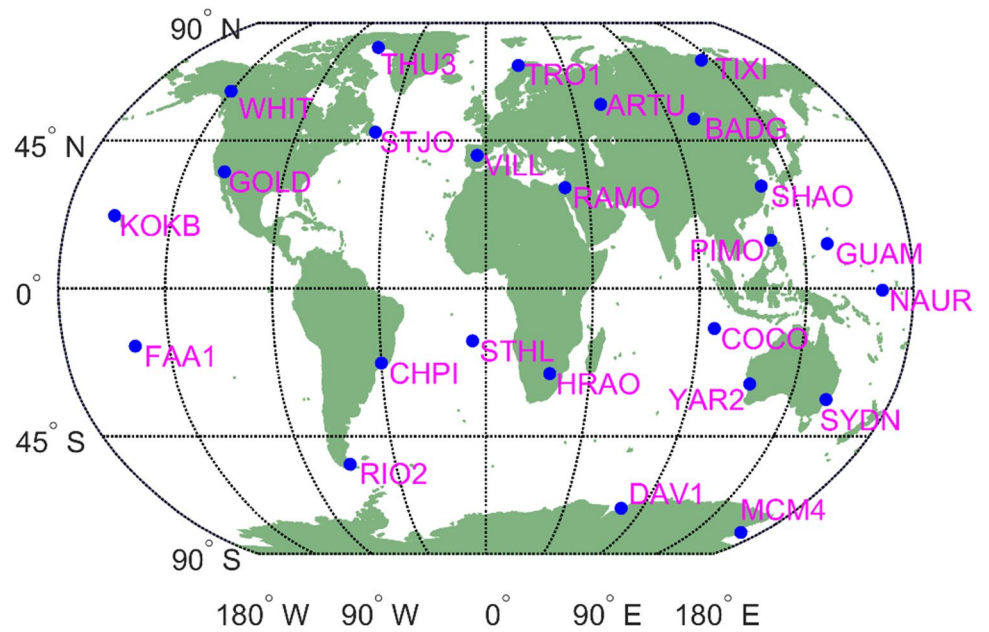
real-time VTEC products, which will be denoted as CNES real-time *STEC* from now on. The evaluation is carried out for Periods 1 and 2 separately and the results are shown in Figs. 8 and 9, respectively. The x-axis labeled as *dSTEC* denotes the error of *STEC* derived from CNES VTEC messages and y-axis labeled as *PDF* presents the probability density function of *STEC* error. It is noted that the plots are ordered according to the latitude from 90° S to 90° N.

For the evaluation of CNES real-time *STEC* in Period 1, the average RMS of the 25 IGS stations is 5.02 TECU. The largest RMS of 7.93 TECU comes from low latitude IGS station FAA1, which is in Tahiti and surrounded by the Pacific, and the smallest RMS is obtained from high latitude IGS station THU3 at 3.02 TECU. For the other high latitude stations such as MCM4, DAV1 and TIXI, the RMS values are smaller than the averaged RMS. Regarding the evaluation in Period 2, the average RMS of the 25 IGS stations is 4.17 TECU. The largest RMS of 6.15 TECU is from the low latitude IGS station KOKB, which in Hawaii and surrounded by the Pacific as well, and the smallest RMS comes from the

**Fig. 6** Time series of bias and RMS for CNES real-time VTEC, and ionospheric Dst index over 374 consecutive days



**Fig. 7** Global distribution of 25 selected IGS stations on the map





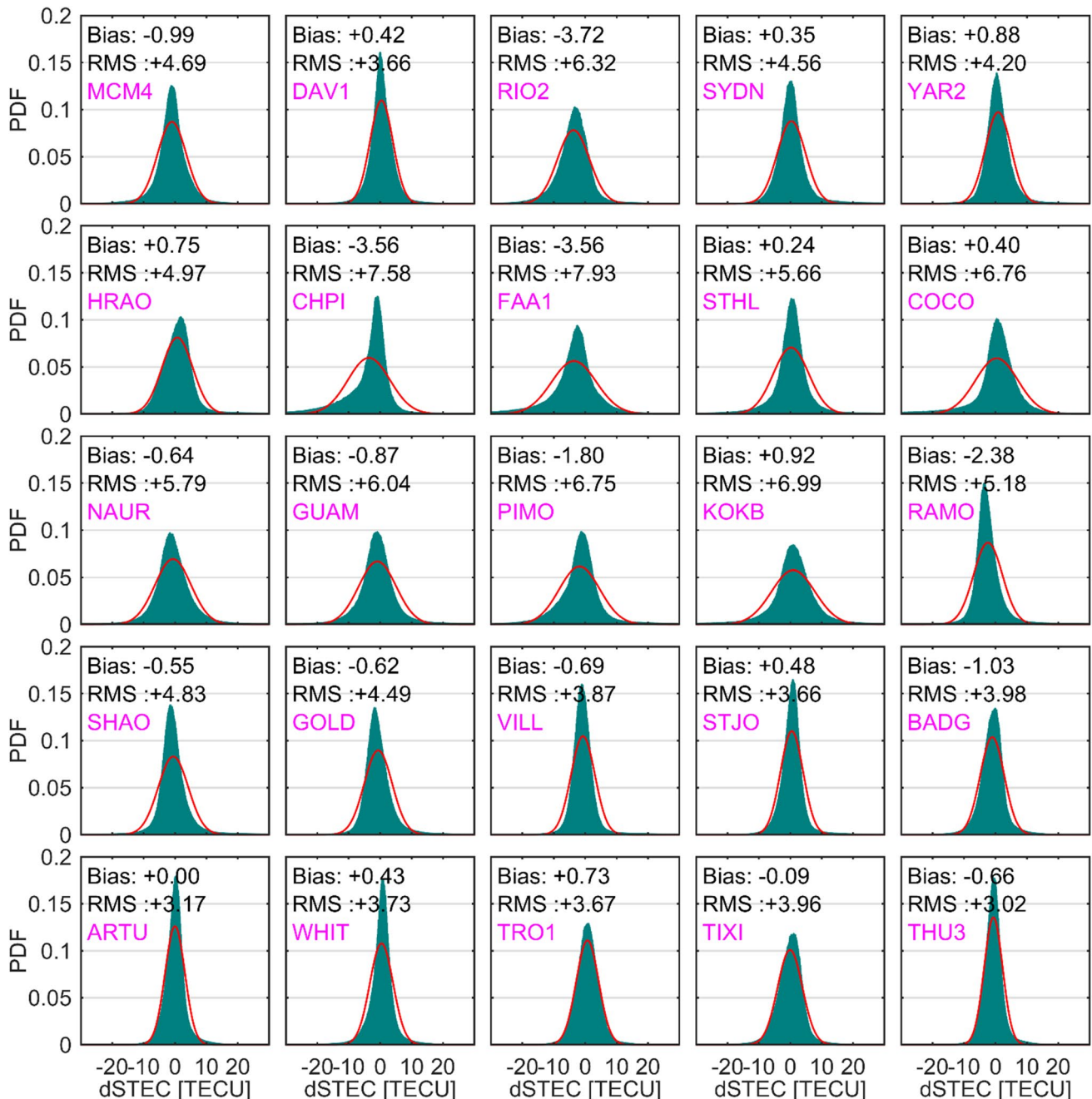


**Fig. 8** Error distribution of the CNES real-time STEC for 25 IGS stations in Period 1

high latitude IGS station MCM4 at 2.07 TECU. For the other high-latitude stations such as DAV1 and THU3, the RMS is also very small at 2.45 and 2.85 TECU correspondingly.

When comparing the evaluation results between Periods 1 and 2, most stations see improvements in RMS, which indicates the quality of real-time ionospheric product increases using VTEC message with the higher degree and order of the spherical harmonic expansions. For CHPI, the RMS reduced from 7.58 TECU in Period 1 to 4.35 TECU in Period 2, and

the improvement of 3.23 TECU is largest among all the stations. Meanwhile, the stations such as MCM4 and RIO2 also show improvements of over 2 TECU. The improvements for stations DAV1, FAA1, STHL, COCO and PIMO are between 1 and 2 TECU, and the improvements for stations YAR2, GUAM, KOKB and TRO1 are between 0.5 and 1 TECU. For the other stations such as SYDN, HRAO, NARU, RAMO, SHAO, GOLD, VILL, STJO, BADG, ARTU, WHIT, TIXI and THU3, the RMS difference in Period 1 and Period 2 are

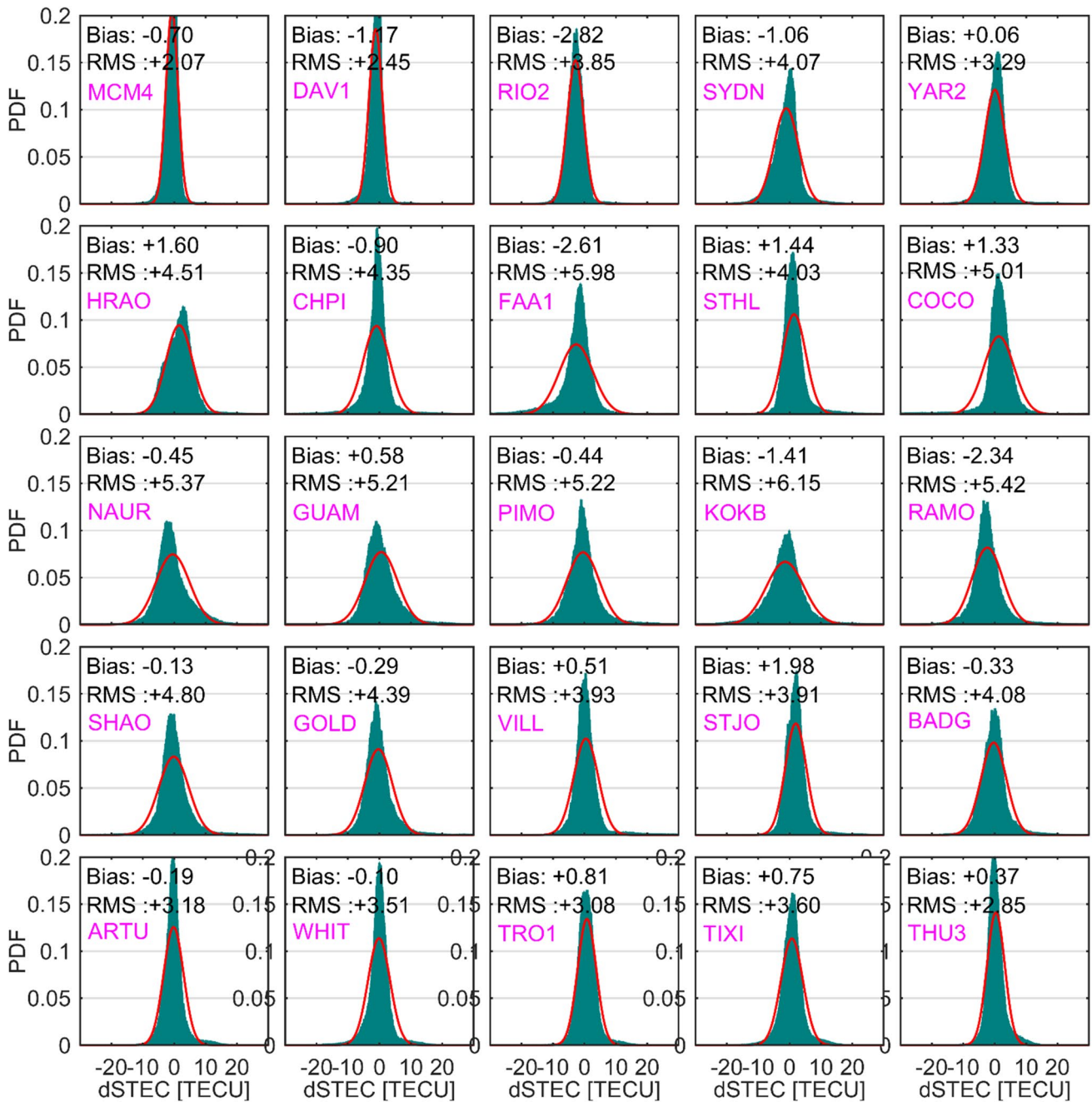


Fig. 9 Error distribution of the CNES real-time STEC for 25 IGS stations in Period 2

less than 0.5 TECU. Generally, the RMS of CNES real-time STEC for low latitude stations is larger than middle and high latitude stations in both periods. Meanwhile, the stations near the oceans or located in ocean areas such as KOKB, FAA1 and COCO see large RMS of CNES real-time STEC in both periods, which can be attributed to the sparse reference stations in these areas. With sparse nearby reference stations, the ionospheric activities may not be accurately modeled by the global spherical harmonic expansion model.

**Performance analysis of real-time single-frequency PPP**

The RT-SF-PPP is carried out to investigate the quality of CNES real-time VTEC products in the positioning domain. The first experiment uses GNSS data from the 25 static IGS stations shown in Fig. 7 over 374 consecutive days. The second experiment is the kinematic field test carried out in Calgary. For both static and kinematic tests, the processing mode is set as kinematic, and both GPS and GLONASS

**Fig. 10** Positioning RMS in east, north and vertical direction for 25 IGS stations in Period 1

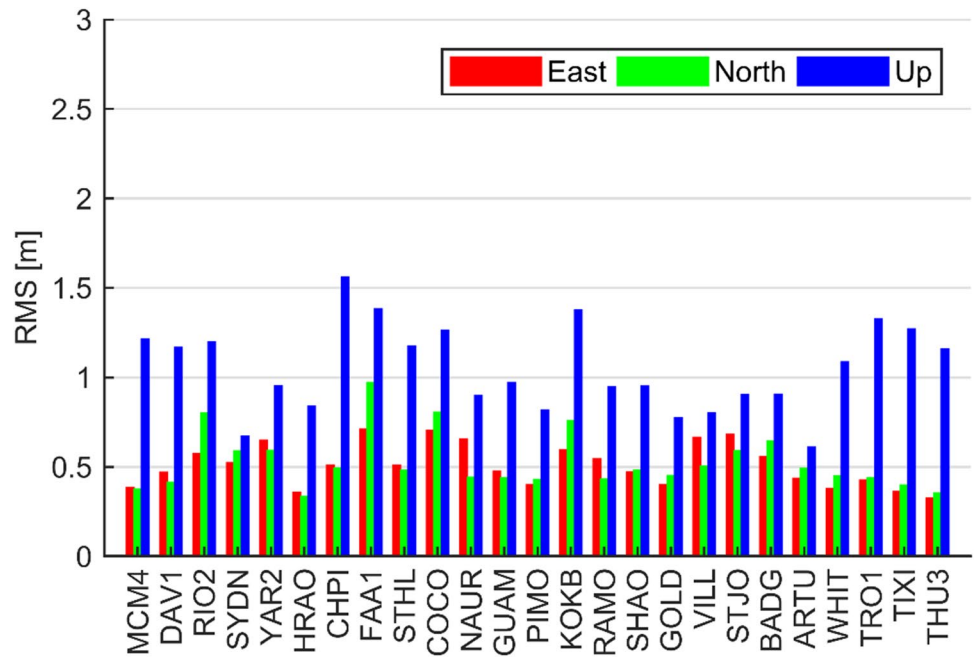
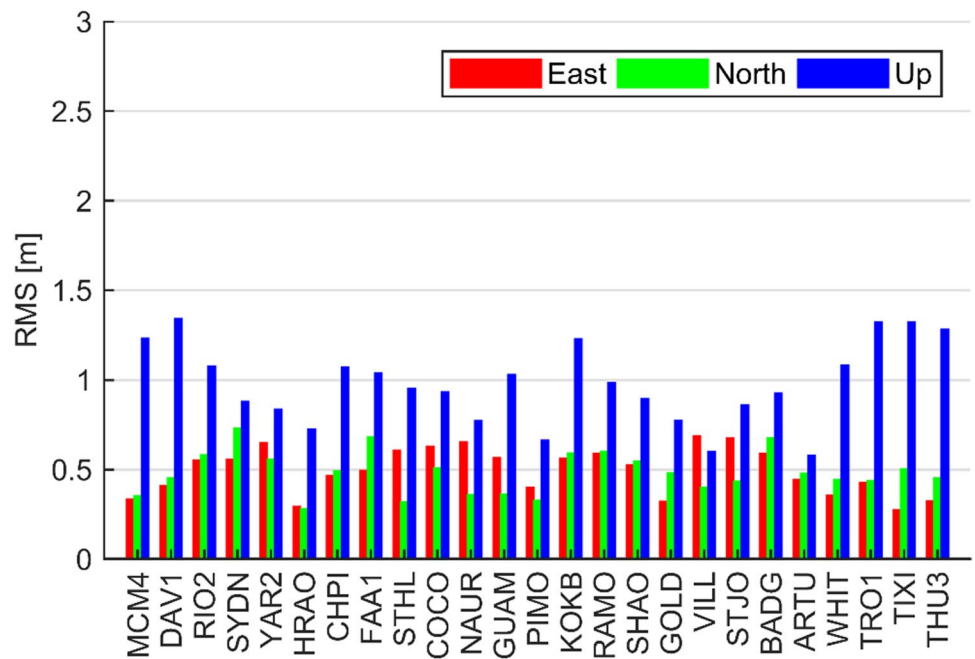


**Fig. 11** Positioning RMS in east, north and vertical direction for 25 IGS stations in Period 2



observations are applied for the positioning. The positioning model and strategies can be referred to de Bakker and Tiberius (2017).

**Stationary experiment and results**

The quality of the CNES real-time VTEC products is assessed in RT-SF-PPP at 25 IGS stations from June 22, 2017 to June 30, 2018. Note that RT-SF-PPP is simulated

by processing the GNSS data in the post mode. The precise coordinates of 25 IGS stations from the IGS weekly SINEX solutions are used as references. Figures 10 and 11 show the positioning accuracy of RT-SF-PPP for the 25 IGS stations in Period 1 and Period 2, respectively.

Generally, using CNES real-time VTEC products, the positioning accuracy of sub-meter-level in the horizontal and meter-level in the vertical direction can be achieved in RT-SF-PPP. For RT-SF-PPP with CNES real-time VTEC

products in Period 1, the average RMS in the east, north, and up directions are 0.507, 0.523, 1.046 m. The RMS in the horizontal direction varies from 0.475 to 1.220 m, and the average is 0.731 m for 25 stations. FAA1 located in Tahiti gets the largest horizontal RMS at 1.200 m, which is due to the sparse nearby reference stations. The station COCO is the only other station with a horizontal RMS of larger than 1 m, which is also due to the location and sparse surrounding reference stations. The RMS in the vertical direction ranges from 0.606 to 1.556 m, and the average is 1.046 m. There are four stations, namely CHPI, FAAI, KOKB and TRO1, with a vertical RMS of more than 1.300 m. For RT-SF-PPP with CNES real-time VTEC products in Period 2, the average RMS values in the east, north, and up directions are 0.492, 0.479, 0.974 m. The RMS in the horizontal direction varies from 0.401 to 0.914 m, and the average is 0.695 m.

The RMS in the vertical direction ranges from 0.577 to 1.338 m, and the average is 0.974 m. When comparing the RT-SF-PPP in Periods 1 and 2, the RMS improvement in the horizontal direction is 0.036 m by averaging all the 25 stations. For stations such as RIO2, FAA1, COCO and KOKB, the improvement of horizontal RMS is more than 0.010 m. The RMS improvement in the vertical direction is 0.072 m by averaging all the 25 stations. For some stations such as CHPI, FAA1, STHL and COCO, the improvement of vertical RMS is more than 0.020 m.

**Automotive experiment and results**

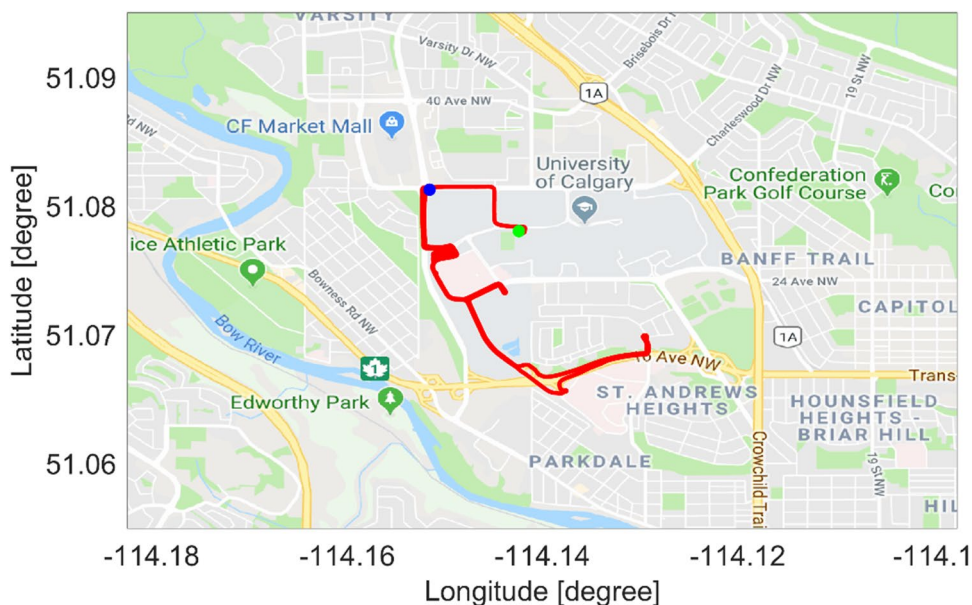
The field test with RT-SF-PPP is conducted from GPST 17:45:05 to 18:45:26 of November 10, 2017 near the University of Calgary, Canada. A u-blox M8T-EVK is connected to a patch antenna mounted on the top of the vehicle, and an Internet-accessible laptop is used to receive u-blox single-frequency observations, CNES real-time products and to conduct RT-SF-PPP. The patch antenna is placed in the middle point of two NovAtel antennas, which are connected to two NovAtel receivers to collect the GNSS data for the generation of reference. RTK is carried out by taking the GNSS data collected by NovAtel receivers as the rover station, and the base station is the UCAL station within 5 km and located inside the University of Calgary. Then the reference is generated by averaging the two RTK solutions from the pair of NovAtel receivers. Note that the height difference has been measured and considered. The location plan of the antennas on top of the vehicle is shown in Fig. 12.



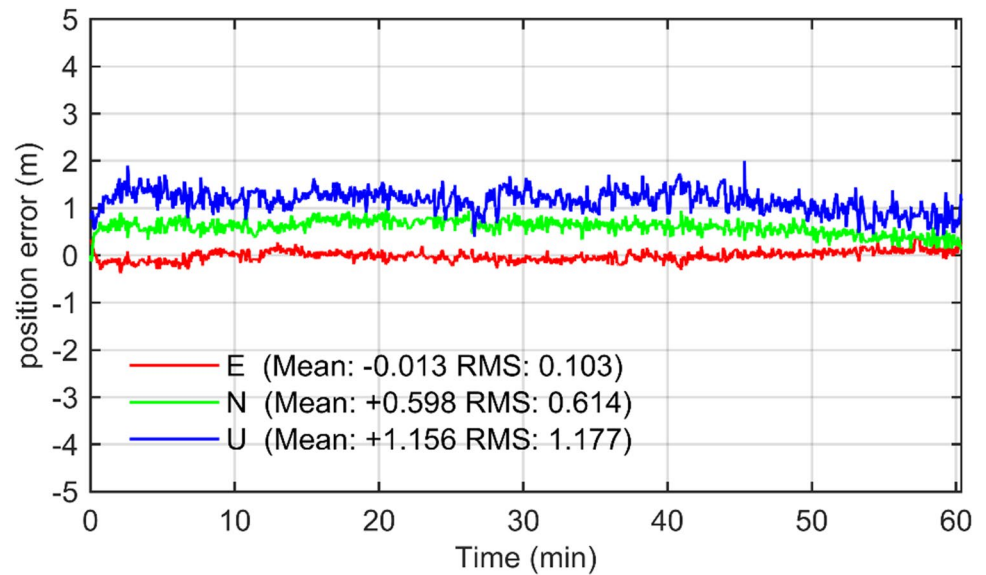
**Fig. 12** NovAtel and patch antennas mounted on top of the land vehicle used in the field test

Figure 13 shows the trajectory derived from the reference and the vehicle speed is less than 60 km/h for the whole trajectory. The positioning errors in east, north and vertical

**Fig. 13** Trajectory of the field test, which starts from the green point and ends at the blue point



**Fig. 14** Positioning errors in east, north and vertical directions of the field test



directions are shown in Fig. 14. We can see that sub-meter level and meter-level accuracy can be achieved in horizontal and vertical, respectively. The RMS values are 0.103, 0.614 and 1.177 m in the east, north and vertical directions, respectively.

## Conclusions

The quality of real-time ionospheric products is essential to the performance of real-time single frequency PPP. In this study, the quality of CNES real-time VTEC products is fully assessed by directly comparing with the IGS final VTEC GIM products, and comparison of STEC values between those computed with CNES VTEC message and those derived from dual-frequency GNSS measurements. RT-SF-PPP is further conducted for assessing the quality of CNES real-time VTEC products in the positioning domain.

To assess the quality of real-time VTEC products, the CNES CLK93 RTS corrections between June 22, 2017 and June 30, 2018 are collected. The availability of the collected VTEC messages is 97.38%, and the degree and order of the spherical harmonic expansions broadcasted in the CNES VTEC messages changes from 6 to 12 during the time span of collected data. During the period from 06:35:00 June 22, 2017 to 07:58:00 May 29, 2018 (Period 1), the spherical harmonic degree and order are both 6, whereas during the period from 08:50:00 May 29, 2018 to 23:59:00 June 30 (Period 2), the degree and order of the spherical harmonic expansions are both 12. With IGS final VTEC GIM products as references, the bias of CNES real-time VTEC varies from  $-3.15$  to  $-0.03$  TECU at different grid points and the RMS varies from 1.06 to 4.91 TECU for Period 1, and the bias varies from  $-2.82$  to 0.06 TECU and the RMS varies

from 0.97 to 3.01 TECU for Period 2. Using STEC values derived from dual-frequency GNSS measurements as references, the bias of STEC computed with CNES VTEC varies from  $-3.72$  to 0.92 TECU among 25 globally distributed IGS stations and the RMS varies from 3.02 to 7.93 TECU for period 1, and the bias and RMS vary from  $-2.82$  to 1.98 TECU and from 2.07 to 6.15 TECU, respectively, for Period 2. From the comparison of real-time VTEC products with IGS final GIM products, and the comparison of STEC between those computed with VTEC message and those derived from dual-frequency GNSS measurements, we confirmed that the quality of real-time VTEC products is highly correlated with latitude. It shows generally better quality in middle latitude and high latitude areas than in low latitude areas. Furthermore, the real-time ionospheric products are also better for correcting ionospheric delay in stations with dense reference networks compared to those near the oceans or located in the ocean areas. Therefore, it is recommended using the real-time ionospheric products with care in low latitude, and near oceans or in ocean areas. It is also noted that the quality of real-time ionospheric products improves using VTEC messages with higher degree and order of the spherical harmonic expansions, especially in the low latitude areas. Higher degree and order ionospheric models are, therefore, desired for more accurate modeling of the ionosphere at a global scale.

RT-SF-PPP experiments were performed at 25 globally distributed IGS stations for further assessment of the real-time ionospheric products. The positioning accuracy of low latitude stations is generally poorer than middle latitude stations. Meanwhile, the positioning accuracy for the inland stations with denser reference stations nearby is better than those stations near oceans or located in the ocean areas. The average RMS values in the east, north and up directions are

0.507, 0.523, 1.046 m in Period 1, while the respective values are 0.492, 0.479, 0.974 m for Period 2. When comparing the RT-SF-PPP in Periods 1 and 2, the RMS improvements are 0.036 and 0.072 m in the horizontal and vertical direction by averaging all the 25 stations. Larger improvement can be seen at the stations in the low latitude region, near oceans or located in ocean areas. Furthermore, a kinematic automotive experiment using a low-cost single-frequency receiver was also conducted to evaluate the performance of RT-SF-PPP. It is demonstrated that the positioning accuracies are 0.614, 0.103, and 1.177 m in the east, north and up directions, respectively. Therefore, it is concluded that the CNES real-time ionospheric products can be used for deriving sub-meter horizontal and meter-level vertical positioning solutions with RT-SF-PPP.

**Acknowledgements** This study was supported by Key Program of National Natural Science Foundation of China (Grant No.: 41631073), National Natural Science Foundation of China (Grant No.: 41604027) and Qingdao National Laboratory for Marine Science and Technology (Grant No.: QNLM2016ORP0401). The authors acknowledge Denis Laurichesse from CNES for valuable discussions. CNES and IGS are thanked for providing the experiment data. In addition, the anonymous reviewers are greatly thanked for their remarks and suggestions.

## References

- Bishop G, Klobuchar J, Doherty P (1985) Multipath effects on the determination of absolute ionospheric time delay from GPS signals. *Radio Sci* 20(3):388–396
- Bisnath S, Gao Y (2009) Current state of precise point positioning and future prospects and limitations. In: Sideris MG (ed) *Observing our changing earth*, vol 133. Springer, Berlin International Association of Geodesy Symposia
- Brunini C, Azpilicueta FJ (2009) Accuracy assessment of the GPS-based slant total electron content. *J Geodesy* 83(8):773–785
- Campbell WH (1996) Geomagnetic storms, the Dst ring-current myth and lognormal distributions. *J Atmos Terr Phys* 58(10):1171–1187
- Choy S (2009) An investigation into the accuracy of single frequency PPP. Dissertation, RMIT University, Australia
- Choy S, Bisnath S, Rizos C (2017) Uncovering common misconceptions in GNSS precise point positioning and its future prospect. *GPS Solutions* 21(1):13–22
- de Bakker PF, Tiberius CCJM (2017) Real-time multi-GNSS single-frequency precise point positioning. *GPS Solutions* 21(4):1791–1803
- Feltens J (2003) The activities of the ionosphere working group of the International GPS Service (IGS). *GPS Solutions* 7(1):41–46
- Gao Y, Zhang Y, Chen K (2006) Development of a real-time single-frequency precise point positioning system and test results. In: *Proc. ION GNSS 2006*, Institute of Navigation, Fort Worth, Texas, USA, Sept. 26–29, pp 2297–2303
- Hadas T, Bosty J (2015) IGS RTS precise orbits and clocks verification and quality degradation over time. *GPS Solutions* 19(1):93–105
- Hernández-Pajares M, Juan JM, Sanz J, Quesada R, García-Rigo A, Feltens J, Komjathy A, Schaer SC, Krankowski A (2009) The IGS VTEC maps: a reliable source of ionospheric information since 1998. *J Geodesy* 83(3–4):263–275
- Hernández-Pajares M, Roma-Dollase D, Krankowski A, García-Rigo A, Orús-Pérez R (2017) Methodology and consistency of slant and vertical assessments for ionospheric electron content models. *J Geodesy* 91(12):1405–1414
- Holmes SA, Featherstone WE (2002) A unified approach to the Clenshaw summation and the recursive computation of very high degree and order normalised associated Legendre functions. *J Geodesy* 76(5):279–299
- Kazmierski K, Sośnica K, Hadas T (2018) Quality assessment of multi-GNSS orbits and clocks for real-time precise point positioning. *GPS Solutions* 22:11. <https://doi.org/10.1007/s10291-017-0678-6>
- Nie Z, Gao Y, Wang Z, Ji S, Yang H (2018) An approach to GPS clock prediction for real-time PPP during outages of RTS stream. *GPS Solutions* 22:14. <https://doi.org/10.1007/s10291-017-0681-y>
- Roma D, Hernandez M, Garcia-Rigo A, Laurichesse D, Schmidt M, Erdogan E, Yuan Y, Li Z, Gómez-Cama JM, Krankowski A (2016) Real time global ionospheric maps: a low latency alternative to traditional GIMs. 19th International Beacon Satellite Symposium (BSS 2016), Trieste, Italy, 27 June–1 July, p 1
- RTCM Special Committee (2014) Proposal of new RTCM SSR Messages, SSR Stage 2: Vertical TEC (VTEC) for RTCM Standard 10403.2 Differential GNSS (Global Navigation Satellite Systems) Services-Version 3. RTCM Special Committee No. 104, USA
- RTCM Special Committee (2016) RTCM Standard 10403.3 differential GNSS (Global Navigation Satellite Systems) Services-Version 3. RTCM Special Committee No. 104, Arlington, TX, USA
- Schaer S (1999) Mapping and predicting the Earth's ionosphere using the Global Positioning System. Dissertation, University of Berne, Switzerland
- Shi C, Gu S, Lou Y, Ge M (2012) An improved approach to model ionospheric delays for single-frequency precise point positioning. *Adv Space Res* 49(12):1698–1708
- Teunissen P, Khodabandeh A (2015) Review and principles of PPP-RTK methods. *J Geodesy* 89(3):217–240
- van Bree RJ, Tiberius CC (2012) Real-time single-frequency precise point positioning: accuracy assessment. *GPS Solutions* 16(2):259–266
- Wang L, Li Z, Ge M, Neitzel F, Wang Z, Yuan H (2018) Validation and assessment of multi-gnss real-time precise point positioning in simulated kinematic mode using IGS real-time service. *Remote Sens* 10(2):337
- Weber G, Mervart L, Lukes Z, Rocken C, Dousa J (2007) Real-time clock and orbit corrections for improved point positioning via NTRIP. *Proc. ION GNSS 2007*, Institute of Navigation, Fort Worth, TX, USA, Sept 25–28, 1992–1998
- Zumberge J, Heflin M, Jefferson D, Watkins M, Webb FH (1997) Precise point positioning for the efficient and robust analysis of GPS data from large networks. *J Geophys Res Solid Earth* 102(B3):5005–5017



**Zhixi Nie** is a postdoctoral scholar in the Department of Electrical and Computer Engineering at the University of Calgary. He got a Ph.D. degree in Geomatics Engineering from the China University of Petroleum in 2017. His research focuses on multi-constellation GNSS positioning and navigation.



**Hongzhou Yang** is GNSS algorithm designer in Profound Positioning Inc, Calgary, Canada. He got a Ph.D degree in Geomatics Engineering from Department of Geomatics Engineering of University of Calgary in 2018. His research focuses on multi-GNSS real-time PPP.



**Yang Gao** is a Professor in the Department of Geomatics engineering at the University of Calgary. His research expertise includes both theoretical aspects and practical applications of satellite-based positioning and navigation systems. His current research focuses on high precision GNSS positioning and multi-sensor integrated navigation systems.



**Peiyuan Zhou** received his Master's degree from Zhengzhou Institute of Surveying and Mapping in 2016. Currently, he is a Ph.D. student at the University of Calgary, Canada. His research interests include GNSS precise positioning and integrated navigation.



**Zhenjie Wang** is a Professor and Head of the Department of Geomatics, China University of Petroleum. His research focuses are in the estimation theory and its application to multi-sensor positioning and navigation. His current special interests are multi-GNSS precision positioning and underwater acoustic positioning.